IEEE Access
Multidisciplinary | Rapid Review | Open Access Journal

Received July 14, 2018, accepted August 24, 2018, date of publication September 4, 2018, date of current version September 21, 2018.

Digital Object Identifier 10.1109/ACCESS.2018.2868549

Predictive Methodology for Dimensional Path Precision in Robotic Machining Operations

I. IGLESIAS[1,2], J. E. ARES[3], C. GONZÁLEZ-GAYA[1], F. MORALES[1], AND V. F. ROSALES[1]

[1]Department of Manufacturing Engineering, Universidad Nacional de Educación a Distancia, 28040 Madrid, Spain
[2]AIMEN Technology Centre, Department of Industrial Services, Mechatronics Unit, 36410 Porriño, Spain
[3]Department of Production Process Engineering, EEI, Universidad de Vigo, 36310 Vigo, Spain

Corresponding author: I. Iglesias (ivaiglesias@gmail.com)

ABSTRACT Industrial robotics seems to be a technology suitable for flexible and reconfigurable manufacturing systems, and robots are commonly used to perform several industrial tasks, such as material handling, welding, assembly, spray painting, machine tending, and milling. For machining operations in particular, the use of industrial robots becomes a cost-saving and flexible alternative compared to conventional CNC machines, which have restricted working areas that limit the produced shapes. Limited pose and path accuracy restrict the use of industrial robots in machining applications. Machining process forces may cause significant tool center point deviations and chatter due to the heavy mechanical demands. This paper proposes a methodology to predict the path deviations due to the machining process, thus allowing to achieve reasonable precision values for the workpiece. An experimental setup was developed to analyze the real-path deviations for different configurations of robot axes. The analysis intends to characterize the mechanical behavior of the machining robot cell and to identify the appropriate cutting conditions.

INDEX TERMS Robot, machining forces, stiffness, chatter.

I. INTRODUCTION

In robotic machining operations, under certain defined cutting and path conditions the deviation and chatter of the tool will depend heavily on the configuration of the robot's axes [1], [2]. In other words, the deviation of the real path with respect to the programmed path, and the chatter of the tool during the machining operations, depend fundamentally on the interrelation between the stiffness of the robot and the magnitude and direction of the cutting force (see Figure 1).

On the other hand, flexible manufacturing systems based on industrial robots represent an indisputable opportunity to perform machining operations, to automate manufacturing processes traditionally carried out by hand [3], or to provide a less costly alternative to the use of computer numerical control (CNC) equipment [4]–[6].

Previous publications confirm that the study of robots performance considers the detailed mechanics of all the movement axes. Those simulation models provide a series of advantages [5], [7], [8], such as the accuracy of the calculated deviations, but their main disadvantage is the need for heavy computer calculations. The main motivation for this research was to develop a predictive methodology to establish and define a simulation model that i) predicts the dynamic structural performance of an anthropomorphic robot of up to 6 degrees of freedom, and ii) quantifies the deviation of its tool central point (TCP).

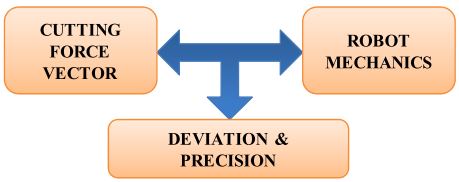

FIGURE 1. Relationship between the cutting constraints and the trajectory deviation.

That would help to correct the robot's stiffness and to select the suitable set of cutting variables that relate to soft materials [9]–[11], both metallic and non-metallic.

II. PREDICTIVE METHODOLOGY

As seen in Figure 2, this methodology to predict machining path deviations focuses on the issue of the robot's structural dynamics regarding the TCP of the cutting tool. This allows evaluating and comparing the deviations between different structural configurations of the robot, aiming to select the

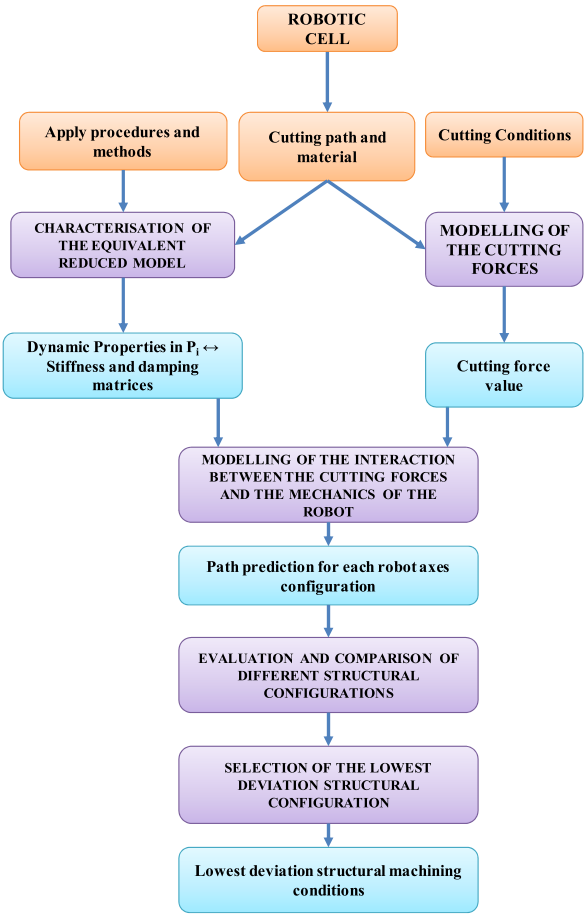

FIGURE 2. Diagram of the predictive methodology.

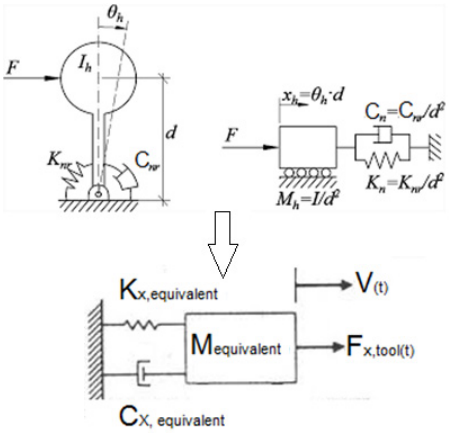

FIGURE 3. Equivalence between the linear and torsional stiffness and damping factors.

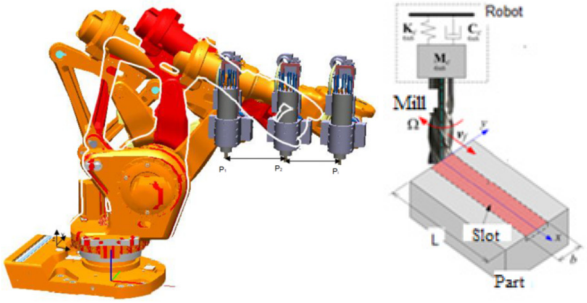

FIGURE 4. Analogue representation of an ABB IRB 6660 robot [12].

cutting path with the least deviation. The predictive methodology consists of the following stages:

Stage 1: Characterization of the reduced equivalent model.

The mechanics of the robot are represented using a reduced equivalent model, and they are characterized for a specific robotic cell by using different techniques and procedures, irrespective of the cinematic features of the robot. In this way, the dynamic properties are obtained at the path points P_i, with the possibility to extend those to the robot's working space by determining the stiffness and damping matrices. The problem focuses exclusively on the study of the dynamic performance of the robot's TCP by presenting a reduced model that might be easily solved within the production environment itself. Figure 3 shows the simplification made based on the equivalence between the linear and torsional stiffness and damping factors for each axes.

To determine the Kr -stiffness- and Cr -damping- matrices, a method has been developed based on the physical principles of damped oscillations, consisting on a linear system with an elastic spring and a viscous damper for each direction of the tool's TCP taken as the hypothesis, as seen in Figure 4.

In this method, the equation that governs the performance of the robot's virtual model is reduced to a one-off dynamic model (TCP) in Cartesian space:

$$[\boldsymbol{M_r}(\boldsymbol{P_i}, \boldsymbol{\theta_1 \ldots, \theta_i})]\left[\ddot{\boldsymbol{X}}\right] + [\boldsymbol{C_r}(\boldsymbol{P_i}, \boldsymbol{\theta_1} \ldots, \boldsymbol{\theta_i})]\left[\dot{\boldsymbol{X}}\right] + [\boldsymbol{K_r}(\boldsymbol{P_i}, \boldsymbol{\theta_1 \ldots, \theta_i})][\boldsymbol{X}] = \boldsymbol{O} \quad (1)$$

where

- M_r (P_i, $\theta_{1\ldots}$, θ_i) is the equivalent matrix of the mass of the robot's axes and machining head obtained using reduction techniques [14] for a specific point P_i of the space with a defined configuration of the robot axes,

$$[\boldsymbol{M_r}(\boldsymbol{P_i}, \boldsymbol{\theta_1} \ldots, \boldsymbol{\theta_i})] = \frac{1}{x_{tcp}^2 + y_{tcp}^2 + z_{tcp}^2} \sum_{i=0}^{N} \boldsymbol{m_i} \times \begin{bmatrix} y_i^2 + z_i^2 & -x_i y_i & -x_i z_i \\ -x_i y_i & x_i^2 + z_i^2 & -y_i z_i \\ -x_i z_i & -y_i z_i & x_i^2 + y_i^2 \end{bmatrix} \quad (2)$$

- K_r (P_i, $\theta_{1\ldots}$, θ_i) is the stiffness matrix equivalent to the mechanical structure of the robot for a point P_i of the space and configuration of the robot axes in Cartesian coordinates focused on the tool's TCP. This matrix considers both the linear and torsional stiffnesses, and
- C_r (P_i, $\theta_{1\ldots}$, θ_i) is the damping equivalent to the mechanical structure of the robot for a specific point P_i of the work space configuration of the robot axes in Cartesian

coordinates focused on the tool's TCP while considering the linear and torsional damping. The Rayleigh damping matrix is used, considering that the damping is proportional to mass and stiffness, where the coefficients a_o and a_1 are calculated from the modal damping factor of two known vibration modes.

$$[\boldsymbol{C_r}(\boldsymbol{P_i}, \boldsymbol{\theta_1} \ldots, \boldsymbol{\theta_i})] = \boldsymbol{a_0}[\boldsymbol{M_r}(\boldsymbol{P_i}, \boldsymbol{\theta_1} \ldots, \boldsymbol{\theta_i})] + \boldsymbol{a_1}[\boldsymbol{K_r}(\boldsymbol{P_i}, \boldsymbol{\theta_1} \ldots, \boldsymbol{\theta_i})] \quad (3)$$

To determine the K_r stiffness matrix, the TCP deviations are evaluated under the action of a known static force by taking displacement measurements using a deflection gauge. To calculate the damping matrix C_r, the acceleration and position of the TCP to which an external force is applied-hammer impact test- until the new equilibrium position is reached is registered using an accelerometer and a digital deflection indicator (see Figure 5).

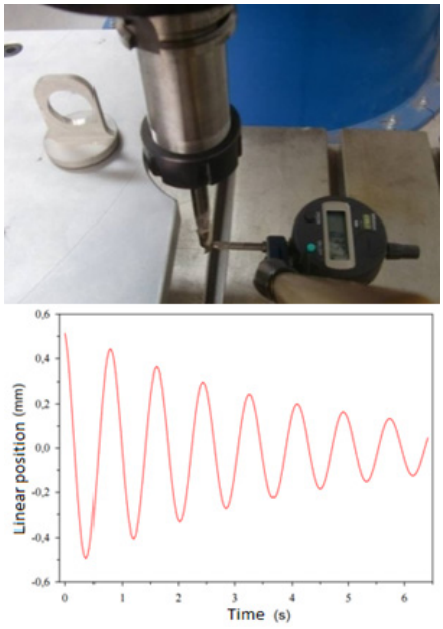

FIGURE 5. Diagram and basic formulation.

Stage 2: Modeling of the cutting forces.

The characteristic cutting-force vector model for the machining process to be carried out, when coupled to the reduced equivalent model, enables the forecasting of the TCP's deviation. To simulate the removal of material, the standard cutting force model based on Altintas is used [14]. This approach disregards the lag time that is responsible for the self-induced chatter during the shaping process, where the geometry of the shaving is defined by the angular thickness h(φ,z) with φ_{in} and φ_{out} being the entry and exit angles respectively (see Figure 6). Since the thickness of the shaving varies along the cutting edge, it will be subdivided into disks of height dz and angle dφ.

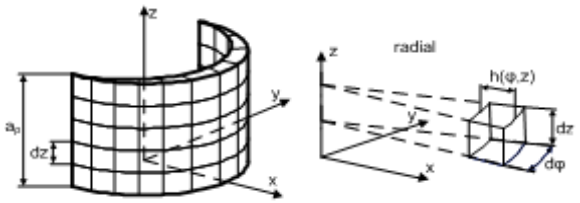

FIGURE 6. Geometry of a shaving.

In accordance with the discretization of the cutting tool geometry, slices of thickness dz are partitioned from it (see Figure 7).

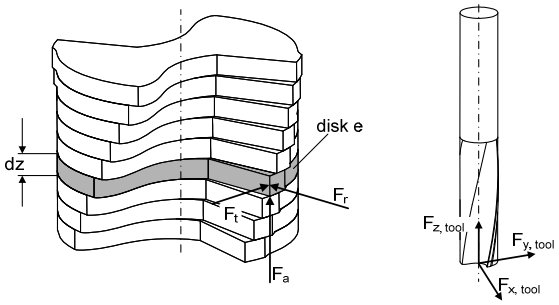

FIGURE 7. Resulting force on the TCP.

For each disk e, $\boldsymbol{F}_{rta,j}$ represents the force due tothe 'j' tooth in the radial, tangential and axial directions.

$$\boldsymbol{F}_{rta,j,e} = \boldsymbol{K}_c dz \boldsymbol{h}_j(\boldsymbol{\varphi}, z) + \boldsymbol{K}_e dz \quad (4)$$

The corresponding shaving thickness $h_j(\varphi,z)$ is inserted depending on the angular position j of the tooth of a slice. The cutting force coefficients $\boldsymbol{K}_c = [K_{rc}, K_{tc}, K_{ac}]$ and $\boldsymbol{K}_e = [K_{re}, K_{te}, K_{ae}]$ are identified beforehand.

The equation for calculating the force $\boldsymbol{F}_{xyz,tool}$ that acts on the TCP of the given tool with respect to a non-rotary coordinate system is obtained from the transformation of $\boldsymbol{F}_{rta,j,e}$ using $\boldsymbol{T}(\varphi)$ and the resulting sum that considers all the teeth N_z and slices N_e.

$$\boldsymbol{F}_{xyz,tool} = \sum_{e=1}^{N_e} \sum_{j=1}^{N_z} \boldsymbol{T}_j(\boldsymbol{\varphi}) \boldsymbol{F}_{rta,j,e} \quad (5)$$

Stage 3: Modeling of the interactions between the cutting forces and the mechanics of the robot.

The deviation of the tool depends on the interaction between the different structural configurations of the robot's mechanics and the cutting parameters. This interaction is calculated from the location of the cutting path and the configuration of the robot's axes. The interaction model predicts the simulated path for a number of structural conditions and cutting parameters which, when compared with the theoretical programmed path, allows the determination of the deviations of the cutting tool's TCP.

The equation that governs the performance of the interaction model applied to a one-off dynamic system (TCP) in

Cartesian space is:

$$[\boldsymbol{M_r}(\boldsymbol{P_i}, \boldsymbol{\theta_1} \ldots, \boldsymbol{\theta_i})]\left[\ddot{\boldsymbol{X}}\right] + [\boldsymbol{C_r}(\boldsymbol{P_i}, \boldsymbol{\theta_1} \ldots, \boldsymbol{\theta_i})]\left[\dot{\boldsymbol{X}}\right] + [\boldsymbol{K_r}(\boldsymbol{P_i}, \boldsymbol{\theta_1} \ldots, \boldsymbol{\theta_i})][\boldsymbol{X}] = \boldsymbol{F_{xyz,tool}} \quad (6)$$

Stage 4: Evaluation and comparison of different structural configurations.

In this stage, the dimensional differences that exist between the simulated path points and the programmed path points-deviations obtained after applying the interaction model-are evaluated. A comparison is made between the geometry obtained from the simulation and the desired geometry for each part location and configuration of the robot's axes. The evaluation of the results is based on identifying the maximum deviation values for each path simulated for their subsequent comparison.

Stage 5: Selection of the lowest-deviation structural configuration.

The final stage of the methodology involves finding out which structural configuration of the robot's mechanics results in a prediction with the lowest simulated path deviation values. Thus, the location of the part and the most suitable configuration of the robot's axes to perform the machining operation are selected.

III. VALIDATION OF THE METHODOLOGY

To validate the methodology proposed in this research, the following apparatuses have been designed:

- A robotic cell, to study the most suitable location of the work table with respect to the stiffness of the robot (see Figure 8).

FIGURE 8. Experimental cell.

- A machining head that enables to study the influences from the configuration or arrangement of the tool on the stiffness of the robot, the weight (W), the position of the gravity center (CG), the inertia, etc. (see Figure 9).

An iterative method is used to calibrate the TCP and the work table. To obtain the calibration values, the Euler angles (α, β, γ) are first measured, there by determining the values

Weight, CG and Virtual TCP	
W	76.534 Kg
CG	X = -5.04 mm Y = 0.30 mm Z = 225.67 mm
TCP	X = 212.50 mm Y = 0 mm Z = 279.91 mm

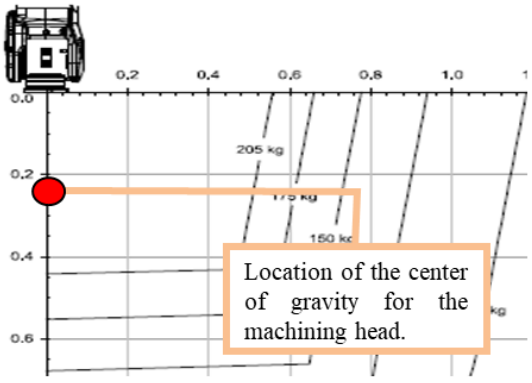

FIGURE 9. Design of the machining head.

of the quaternions (q_1, q_2, q_3, q_4) before obtaining the X, Y, and Z positions.

Different alternatives have been evaluated to define the cutting path, and a conclusion has been reached that the slotting operation is the most suitable due to the simplicity it offers to establish the shaving geometry that results from the cutting force (see Figure 10).

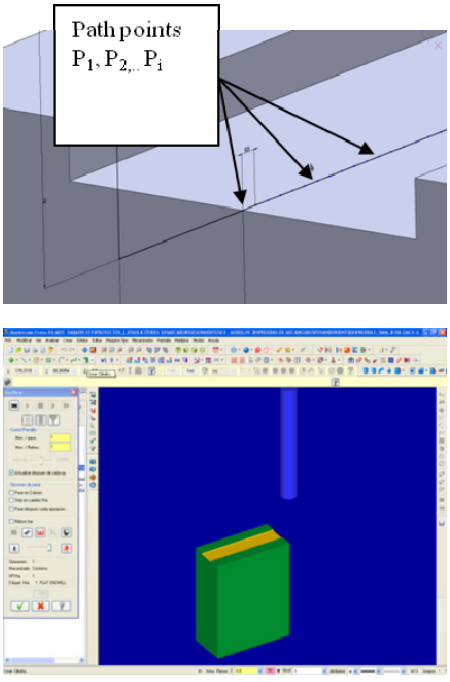

FIGURE 10. Programmed path.

Next, the case study in which the method is applied to two different robot-axes configurations was defined

(see Figure 11 and 12), as was the location of the part itself. Each stage of the methodology will be implemented once the experimental validation conditions have been determined.

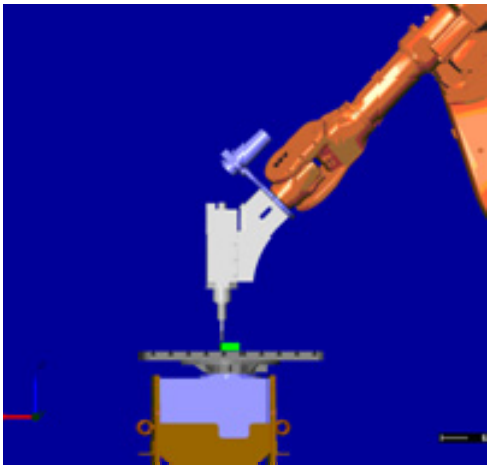

FIGURE 11. Configuration 'A' for the robot's axes.

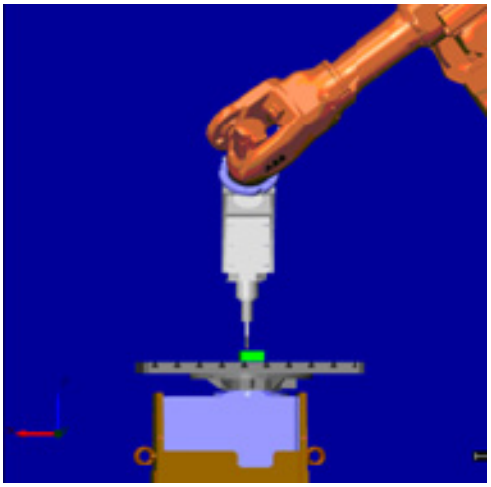

FIGURE 12. Configuration 'B' for the robot's axes.

The reduced equivalent model that represents the robot's mechanics was characterized in stage 1 (Equation 1). The procedure [15] to calculate the mass, stiffness and damping matrices for the configuration 'A' of axes (M_{rA}, K_{rA} and C_{rA}) and for the configuration 'B' of axes (M_{rB}, K_{rB} and C_{rB}) in the different points P_i of the machining path is applied.

The mass matrices $M_{rA and}M_{rB}$ are calculated considering the masses of the mobile elements of the robot (moving axes) and the machining head.

The stiffness matrices K_{rA} and K_{rB} have been calculated by applying 100N and 200N forces, and then measuring the displacements produced. The following table shows the measurement's results for the first 8 trajectory points:

The damping matrices C_{rA} and C_{rB} have been calculated by determining the coefficients a_0(0.9198) and a_1(0.0021) obtained from the vibration modes of the hammer impact test.

TABLE 1. TCP deviation values.

Path point	Fx_1 (N)	Dx_1 (mm)	Dy_1 (mm)	Dz_1 (mm)	Fx_2 (N)	Dx_2 (mm)	Dy_2 (mm)	Dz_1 (mm)
P1	100	0,34	0,008	0,007	200	0,600	0,020	0,009
P2	100	0,345	0,020	0,011	200	0,625	0,041	0,016
P3	100	0,343	0,03	0,008	200	0,625	0,048	0,018
P4	100	0,34	0,009	0,009	200	0,651	0,06	0,020
P5	100	0,34	0,054	0,013	200	0,695	0,078	0,019
P6	100	0,38	0,020	0,021	200	0,745	0,06	0,031
P7	100	0,395	0,033	0,003	200	0,765	0,07	0,013
P8	100	0,475	0,027	0,007	200	0,825	0,067	0,004

An example of the results obtained are the following matrices:

$$M_{rA} = \begin{bmatrix} 653.59 & 0 & -381.51 \\ 0 & 904.38 & 0 \\ -381.51 & 0 & 268.57 \end{bmatrix}$$

$$M_{rB} = \begin{bmatrix} 650.36 & -5.1 & -379.43 \\ -5.1 & 917.41 & -3.82 \\ -379.43 & -3.82 & 267.11 \end{bmatrix}$$

$$K_{rA} = \begin{bmatrix} 3.31 & 0 & 0 \\ 0 & 7.13 & 0 \\ 0 & 0 & 8.72 \end{bmatrix} x10^5$$

$$K_{rB} = \begin{bmatrix} 3.59 & 0 & 0 \\ 0 & 7.45 & 0 \\ 0 & 0 & 8.85 \end{bmatrix} x10^5$$

$$C_{rA} = \begin{bmatrix} 1296.27 & 0 & -350.91 \\ 0 & 2329.15 & 0 \\ -350.91 & 0 & 2078.23 \end{bmatrix}$$

$$C_{rB} = \begin{bmatrix} 1352.1 & -4.69 & -348.99 \\ -4.69 & 2408.33 & -3.51 \\ -348.99 & -3.51 & 2104.19 \end{bmatrix}$$

To model the cutting forces (stage 2) for the slotting operation, an EN AW-5083 aluminum tool with a diameter of 10 mm and cutting parameters of n = 8,000 rpm, v_f = 50 mm/s and a_p = 2 mm was used. The maximum value for the cutting force (Equation 2) was calculated for the P_i path points with a value of 102 N being obtained.

Using the results obtained in the execution of stages 1 and 2, the deviation of the tool in stage 3 due to the interaction between the different structural configurations of the robot's mechanics and the cutting parameters for each Pi path point is predicted. The results of the deviations obtained for the case study show 0.309 mm for configuration 'A' and 0.394 mm for configuration 'B' as the maximum values.

In stage 4, the evaluation of, and the comparison with, the results obtained using configurations 'A' and 'B' are performed, and the differences that exist between each configuration of the robot's axes and the path deviation are shown. The outcome corresponding to configuration 'A' resulted in the lower deviation value obtained.

Using the results obtained in phase 5, the lower-deviation structural mechanical configuration is selected. Based on the path deviation values obtained, it is predicted that the most appropriate configuration of the axes to machine the slots is the 'A' configuration for the robot's axes.

FIGURE 13. Machined aluminum test parts.

Once the best prediction value was identified as the result to apply to the methodology, work began to evaluate the experimental level of the deviation results obtained using the simulation model (see Figure 13). Experimental tests were carried out using the same path programmed in configurations 'A' and 'B' and considered in the simulation model. Thus, the path points were used to determine the stiffness and damping matrices. The path-deviation values calculated in the prediction phase of the methodology were then compared with the deviation values obtained experimentally.

The parts were measured using a coordinate measuring machine. Both sides of the slot were measured to obtain their right- and left-hand profiles, and the maximum deviations in each profile were determined. The path-deviation value chosen was that corresponding to the least-deviation profile. Figure 14 compares the profiles of the minimum path deviation for the case study, where the maximum deviation value for configuration 'A' of the robot's axes (magenta) is 0.411 mm, while for configuration 'B'(blue) it is 0.518 mm.

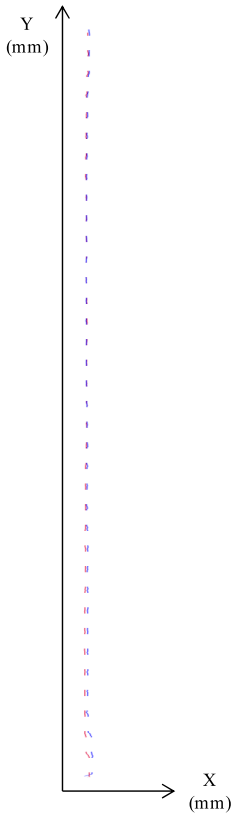

FIGURE 14. Minimum-path deviation profiles.

TABLE 2. Predicted and experimental values.

	Deviation	
	Configuration 'A'	Configuration 'B'
Prediction	0.309	0.394
Experimental with systematic error	0.411	0.518
Experimental with correction factor	0.341	0.448
% Difference	9.38%	12.05%

IV. EVALUATION OF THE PREDICTION AND EXPERIMENTAL RESULTS

The results obtained from the predictions and the experimental tests for the different robot-axes configurations are shown together in the following table.

The experimental results show a quantifiable systematic error corresponding to the repeatability value of the machining robot, which is quantified as 0.07 mm for the robot used. Therefore, to compare the prediction results to the experimental results, the latter must be corrected using some corrective coefficients.

The difference between the results of the deviations from the predictions and the corrected actual experimental deviations are less than 13%, this being an acceptable error level between the prediction and the experimental values, thus validating the implemented and the predictive methodology.

V. CONCLUSIONS

A methodology that enables a reliable prediction for the path of the TCP in robotic-cell machining operations was developed and implemented. It was shown that this simple method requires little computing time to predict the path

deviation of the cutting tool and, therefore, estimates the manufacturing tolerances of the part to be obtained. As a result, the proposed method is an interaction model that relates the robot's mechanics with the cutting forces. In turn, this will enable future users to establish suitable robotic machining production strategies in the workshop.

The main advantage of applying this methodology is that it enables the study of the conditions that influence the most the deviation of the robot's TCP. This was achieved by defining a simulation model that can be used to optimize the anthropomorphic use of the robot by way of selecting the most appropriate cutting conditions. This was accomplished by making the best use of the stiffness of the robot for the material-removal shaping processes, the best orientation of the cutting path and the most suitable positioning of the part.

REFERENCES

[1] Z. Pan, H. Zhang, Z. Zhu, and J. Wang, "Chatter analysis of robotic machining process," *J. Mater. Process. Technol.*, vol. 173, no. 3, pp. 301–309, 2006.

[2] C. Dumas, S. Caro, S. Garnier, and B. Furet, "Joint stiffness identification of six-revolute industrial serial robots," *Robot. Comput.-Integr. Manuf.*, vol. 27, no. 4, pp. 881–888, 2011.

[3] F. Vidal, M. Á. Souto, R. González, and I. Iglesias, "Development of a flexible and adaptive robotic cell for marine nozzles processing," in *Proc. IEEE 17th Int. Conf. Emerg. Technol. Factory Automat. (ETFA)*, Sep. 2012, pp. 1–8.

[4] I. Iglesias, M. A. Sebastián, and J. E. Ares, "Overview of the state of robotic machining: Current situation and future potential," *Procedia Eng.*, vol. 132, pp. 911–917, Jan. 2015.

[5] Y. Chen and F. Dong, "Robot machining: Recent development and future research issues," *Int. J. Adv. Manuf. Technol.*, vol. 66, nos. 9–12, pp. 1489–1497, 2012.

[6] B. Denkena, B. Bergmann, and T. Lepper, "Design and optimization of a machining robot," *Procedia Manuf.*, vol. 14, pp. 89–96, Jan. 2017.

[7] H. Vieler, A. Karim, and A. Lechler, "Drive based damping for robots with secondary encoders," *Robot. Comput.-Integr. Manuf.*, vol. 47, pp. 117–122, Oct. 2017.

[8] J. Bauer *et al.*, "Analysis of industrial robot structure and milling process interaction for path manipulation," in *Process Machine Interactions*. Springer, 2011.

[9] J. DePree, "Robotic machining white paper project," Halcyon Develop.-Robotic Ind. Assoc., Buena Park, CA, USA, Tech. Rep., 2008.

[10] J. Wang, H. Zhang, and T. Fuhlbrigge, "Improving machining accuracy with robot deformation compensation," in *Proc. IEEE Int. Conf. Intell. Robots Syst. (IROS)*, Oct. 2009, pp. 3826–3831.

[11] T. Kubela, A. Pochyly, and V. Singule, "Assessment of industrial robots accuracy in relation to accuracy improvement in machining processes," in *Proc. IEEE Int. Power Electron. Motion Control Conf. (PEMC)*, Varna, Bulgaria, Sep. 2016, pp. 720–725.

[12] A. Klimchik *et al.*, "Compliance error compensation in robotic-based milling," in *Informatics in Control, Automation and Robotics*. Springer, 2014, pp. 197–216.

[13] S. Briot *et al.*, "Reduced elastodynamic modelling of parallel robots for the computation of their natural frequencies," in *Proc. 13th World Congr. Mechanism Mach. Sci.*, Guanajuato, Mexico, 2011, pp. 19–25.

[14] Y. Altintas, *Manufacturing Automation: Metal Cutting Mechanics, Machine Tool Vibrations, and CNC Design*. Cambridge, U.K.: Cambridge Univ. Press, 2000.

[15] I. Iglesias, "Desarrollo de una metodología predictiva de precisión y acabado superficial aplicada al mecanizado robotizado," Ph.D. dissertation, 2016.

I. IGLESIAS, photograph and biography not available at the time of publication.

J. E. ARES, photograph and biography not available at the time of publication.

C. GONZÁLEZ-GAYA, photograph and biography not available at the time of publication.

F. MORALES, photograph and biography not available at the time of publication.

V. F. ROSALES, photograph and biography not available at the time of publication.